On the Validation of Human Body Models with a Driver-in-the-Loop Simulator

Fabian Kempter[1], Jörg Fehr[1], Norman Stutzig[2] and Tobias Siebert[2]

[1] *Institute of Engineering and Computational Mechanics, University of Stuttgart, Germany*
[fabian.kempter,joerg.fehr]@itm.uni-stuttgart.de
[2] *Institute of Sport and Exercise Science, University of Stuttgart, Germany*
[norman.stutzig,tobias.siebert]@inspo.uni-stuttgart.de

ABSTRACT *For the development of modern integrated safety systems, standard simulation models of anthropometric test devices, often called crash test dummies, are inappropriate for Pre-Crash investigations due to missing activation possibilities, tuned characteristics for one specific accident scenario and high passive stiffness properties [1]. To validate safety concepts getting active prior to the crash new tools like suitable virtual models of human occupants are required. Human Body Models (HBM) provide a higher biofidelity and can be equipped with active muscle elements enabling different muscle activation strategies. To improve the muscle activation strategy and the stiffness properties of active HBMs, validation processes on the basis of low-acceleration experiments, i.e. [2], are inevitable. In contrast to Post Mortem Human Surrogates only low-severity tests can be performed with real human subjects. This paper presents the workflow of a validation process based on an academic scale Driver-in-the-Loop (DiL) simulator in combination with a synchronized measurement chain consisting of an Optitrack stereo vision and an electromyography detection system.*

1 Introduction

For the development of passive safety systems, standard simulation models of anthropometric test devices can be used to predict and investigate possible injury risks at specific crash situations. However, these so-called safety dummies are inappropriate for Pre-Crash investigations/simulations due to missing activation capabilities, tuned characteristics for one specific accident scenario and high passive stiffness properties [1]. To validate integrated safety concepts, getting active prior to the crash, an enormous number of different scenarios have to be investigated [3]. Neither real-world driving nor experimental crash-tests will be able to cover these demands. With virtual testing lots of scenarios, crash situations included, can be tested without any risk for human lives. For this purpose, new engineering tools like suitable virtual models of human occupants are required. The importance of Human Body Models (HBM) in the field of crash simulation is increasing. These models provide a higher biofidelity by direct modeling of the musculoskeletal structure of the human body. Equipped with active muscle elements, the kinematics of these active HBMs can be controlled by arbitrary and reflexive controller patterns [4, 2]. Therefore, the behavior of real human occupants can be emulated more accurately than with dummy models, especially in low-acceleration driving situations. The kinematic as well as stiffness properties can be controlled during runtime. To improve the muscle activation strategy and the stiffness properties of current active HBMs, validation processes on the basis of low-acceleration experiments with real subjects, e.g. [2], are inevitable. There are several possibilities to get validation data based on experimental tests with test persons. Possible approaches are basic experimental setups like head fall tests [2], sled tests [5], investigations with real cars [6, 7] and tests using driving simulators [8, 9]. They each have advantages and disadvantages in terms of possible trajectories (size and multi-directionality), reproducibility, transferability to real crash scenarios, interaction with other road users, etc. In homologation procedures of the past only one-directional scenarios like front and side-crashes were taken into

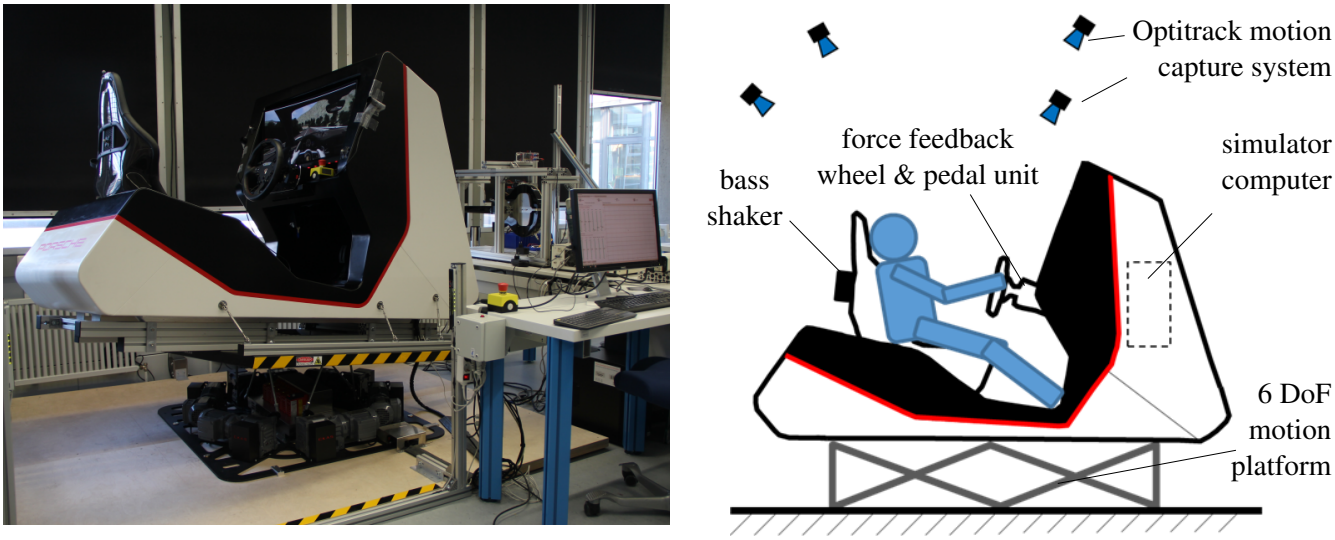

Fig. 1: Setup of the presented Driver-in-the-Loop (DiL) simulator with a Porsche racing simulator, a stewart motion platform and an optitrack motion capture system consisting of four cameras attached to the ceiling.

account. In the future, the focus will be on more realistic and multi-directional crash scenarios in combination with active safety concepts [10, 11]. In this study, a driving simulator approach is taken. This approach enables kinematic feedback in all six degrees of freedom and visual feedback of a virtual driving environment. Furthermore, in contrast to classical sled tests, multi-directional trajectories can be performed with limitations on acceleration and total platform displacements. Other aspects which can be investigated with the DiL-simulators are the interaction of the driver with active safety systems and the estimation of the driver's state. As HBM are suited for simulations of low-g scenarios, they can be validated with scenarios performed by volunteers in a driving simulator. Therefore, this study shows the implementation of a DiL simulator on academic scale, see Fig. 1. It enables access for students and young researchers to get familiar with modern measurement devices included in a workflow for validation processes. Non-standard measurement chains can be implemented and tested without the usual pressure of time when working with commercial high-end driving simulators. With the data obtained in the simulator, active human body models can be validated. Especially muscle activation related topics, like co-contraction at joints to control stiffness properties or type of muscle activation strategies can be investigated. In the following section, the hard- and software of the DiL simulator responsible for kinematic feedback and good driving immersion is given. The measurement chain to detect the behavior of the occupants is explained in Section 3. In Section 4 the first performed tests are explained. Some initial results of these tests are displayed in Section 5 to demonstrate the performance of the total setup. Finally, we conclude this study in Section 6.

2 Layout of the Driver-in-the-Loop Simulator

To perform validation tests, a low-cost Driver-in-the-Loop (DiL) simulator with kinematic feedback in the form of a 6 DoF motion platform, a force-feedback wheel and a bass-shaker at the back of the driving seat is implemented, see Fig. 1 and 2. With the hardware setup the software packages

- ASSETTO CORSA as a racing simulator game or
- PRESCAN as a software package for the simulation and development of ADAS and active safety concepts

can be used, besides others, to enable DiL-simulations.

ASSETTO CORSA provides an all-in-one package for the activation of sound system and force-feedback-wheel. Even the interface between motion platform and ASSETTO CORSA is supported by a Python Plugin. It ensures a high driver immersion by detailed graphics, sound, individual vehicle and platform dynamics with consideration

of road roughness. Due to the main aim of the software as commercial racing game, it does not provide an open control structure to build reproducible crash scenarios and control other road users. However, user-defined tracks can be modeled, i.e. using Blender or other 3D modeling software.

PRESCAN is basically aimed for the development and validation of advanced driving assistance systems (ADASs) including the consideration of sensor signals. Additionally, it allows the implementation of DiL simulations by providing 3D-vehicle models and interfaces for external devices. The basic SIMULINK model generated with the software package PRESCAN includes vehicle models, visualization of the designed scenario and logical operations to ensure reproducible crash scenarios. However, the driver immersion of the standard SIMULINK model is only rudimentary due to the limited graphical illusion, the lack of neither sound support nor plugin for the motion platform. The immersion can be enhanced by additional features which can be connected to the DiL-simulation, i.e. by using udp-communication. Due to the open structure and expandability, we use in the following PRESCAN for defining crash scenarios and the tests for validation of human body models.

2.1 Driver-in-the-Loop Simulation with PRESCAN

To enable DiL-simulations with PRESCAN some interfaces have to be implemented. By extensions of the SIMULINK model with interfaces to external applications, see Fig. 2, the driver immersion can be increased. Mostly udp-communication is used to send information to additional tools calculated on a second device. In total, the DiL simulator provides visual, acoustic, haptic and kinematic feedback for the driver. The coupling of hard- and software is performed in the SIMULINK model generated with PRESCAN version 8.2.0. The DiL-simulaton model is calculated with a framerate of 200 Hz.

2.2 Vehicle model

For the implementation of an interactive Driver-in-the-Loop simulation, an adequate vehicle model is inevitable. The visualization of the scenery as well as the activation of the motion platform is based on the states of the vehicle driven by the test person. For the startup we use the default 3D vehicle model provided by PRESCAN , see Fig. 3. The vehicle controlled by the test person is modeled as a rigid body system with five components. It offers ten degrees of freedom (DoF): six DoF of the main sprung mass representing the chassis and four additional DoF representing the z-displacement of the unsprung mass at each tyre. A basic tyre model is implemented in the

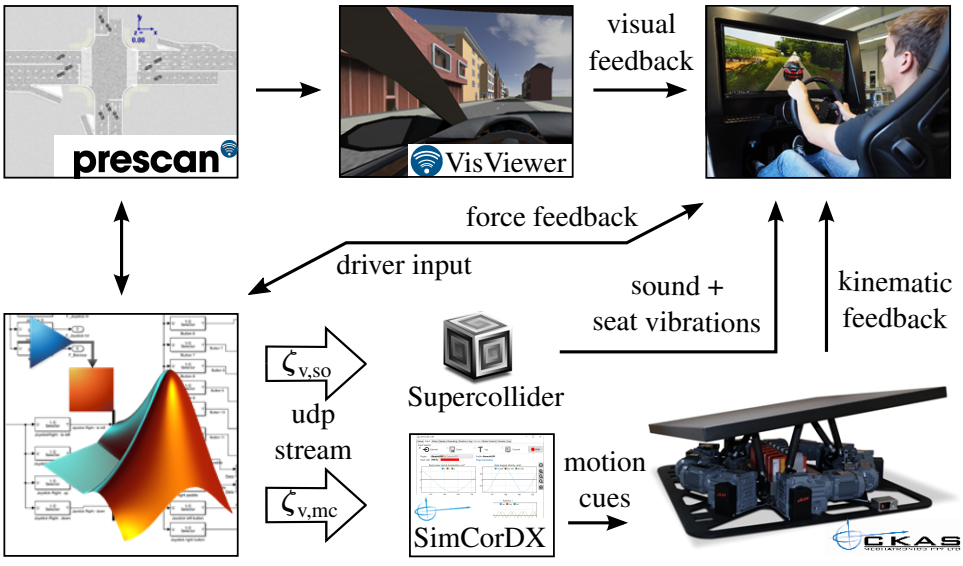

Fig. 2: Workflow of the Driver-in-the-Loop simulator and PRESCAN . The SIMULINK model controls the DiL-simulation with all submodules and thus, ensures the different types of feedback for the driver.

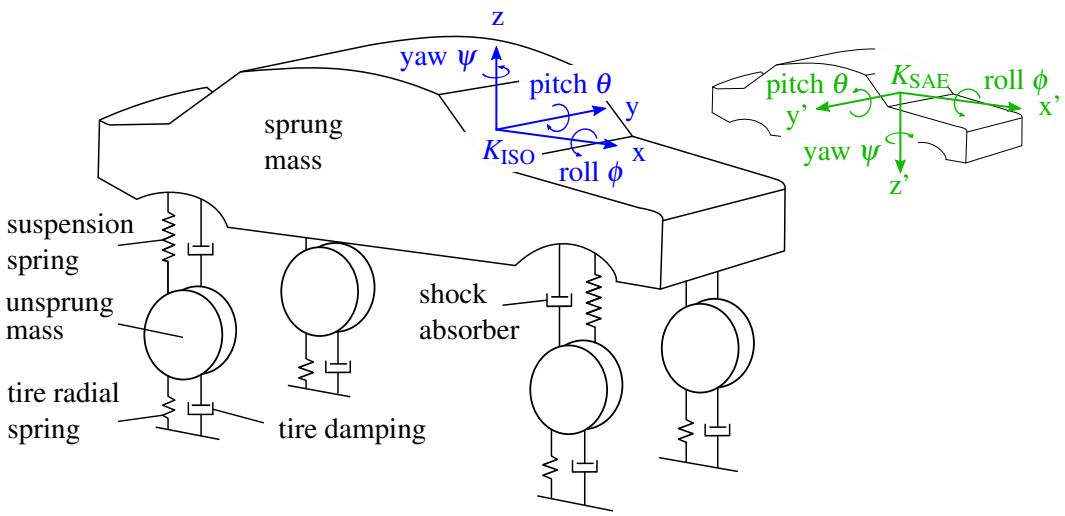

Fig. 3: The simple 3D vehicle model of PRESCAN with ISO coordinate system, see [12]. The alternative SAE convention is depicted in the right top.

PRESCAN model. In future investigations, the vehicle model could be stimulated by road roughness, i.e. by using OPENCRG [13] for description of the road surfaces. However, for the initial test scenarios we do not use any road roughness.

In this study the coordinate system K_{ISO} is used to describe the kinematics of the vehicle as well as the ones of the driver. In this convention, the x-axis is parallel to the vehicle longitudinal axis and points to the driving direction. The z-axis shows upwards.

$$\beta_{\mathrm{veh}} = \begin{pmatrix} \phi \\ \theta \\ \psi \end{pmatrix}_{\mathrm{veh}} \tag{1}$$

To describe the orientation of the vehicle ϕ is used as roll angle, θ as pitch angle and ψ as yaw angle. The transformation is defined by using Tait-Bryan angles with the order roll-pitch-yaw. The transformation matrix between inertial and rotated system is defined as:

$$\mathbf{R}_{\mathrm{IR}} = \mathbf{R}_{\mathrm{xy'z''}} = \mathbf{R}_{\psi}\mathbf{R}_{\theta}\mathbf{R}_{\phi} = \begin{bmatrix} c_\psi c_\theta & c_\psi s_\phi s_\theta - c_\phi s_\psi & s_\phi s_\psi + c_\phi c_\psi s_\theta \\ c_\theta s_\psi & c_\phi c_\psi + s_\phi s_\psi s_\theta & c_\phi s_\psi s_\theta - c_\psi s_\phi \\ -s_\theta & c_\theta s_\phi & c_\phi c_\theta \end{bmatrix} \tag{2}$$

with the local initial axis x and the rotated axes y' and z''.

In contrast to the PRESCAN vehicle model, the platform software SIMCORDX uses the SAE-coordinate system. This alternative coordinate system K_{SAE} differs in the orientation of the y- and z-axis, see Fig. 3. The transformation order is yaw-pitch-roll [14]. For the activation of the motion platform the transformation between the different coordinate systems has to be taken into account, see section 2.4.1.

2.3 Visualization

The driver exposes the visual feedback of the DiL-simulation through a 34" curved screen. The visualization enables interactions with other road users and is one key factor of the immersion rating of the driver. Especially by the peripheral perception, the driver gets a feeling of velocity and distances to obstacles or other cars. This aspect could be satisfied by using additional screens at both sides of the driver to enlarge the viewing angle of the driver. Another approach to enhance the visual driver's immersion is the usage of head mounted displays (HMDs). HMDs further enhance the immersion by disabling the perception of the inertial environment of the lab. In addition, the problem of bad distance estimation within DiL-simulators using standard video projection could be improved by HMDs and serve as alternative to high-cost 3D stereo projection systems, presented in [15]. However, the usage

of HMDs in a non-inertial system leads to some challenges which are subject of further investigations and are out of the scope of this study.

2.4 Kinematic Feedback

To increase the driver immersion inside the DiL-simulator, kinematic feedback is another important component. Especially in combination with virtual reality approaches, like HMDs or projection domes, adequate kinematic feedback is important to reduce the risk of motion sickness [16]. Due to the missing visual information on the inertial reference system, the driver cannot distinguish between the virtual scenery and real-world accelerations. Therefore, the kinematic feedback should fit the visual input as precisely as possible.

The motion platform of the presented simulator only allows movements within the borders of ± 50 *mm*, $\pm 100\ \frac{mm}{s}$, $\pm 0.3\ G$ in translational and $\pm 10^\circ$, $\pm 15^\circ\ s^{-1}$, $\pm 150^\circ\ s^{-2}$ in rotational direction. Due to the limitation in translational movement space, the trajectories of the vehicle model cannot be used directly for platform activation. To provide an adequate kinematic feedback anyway, Motion Cueing Algorithms (MCAs) are commonly used in driving or flight simulators.

2.4.1 Classical Motion Cueing Algorithms

The CKAS W3s motion platform is activated by the software SIMCORDX performing classical Motion Cueing optimized for small simulators [14]. Classical Motion Cueing Algorithms use the three basic approaches: **scaling**, **tilt coordination (TC)** and **washout filtering**. The classical MCAs scale and filter the incoming vehicle states $\boldsymbol{\zeta}_{\text{veh}}$, consisting of values of acceleration $\mathbf{a}_{\text{veh}}$, orientation $\boldsymbol{\beta}_{\text{veh}}$ and angular velocity $\dot{\boldsymbol{\beta}}_{\text{veh}}$, and calculate adequate translational $\mathbf{s}_{\text{p}}$ and rotational $\boldsymbol{\beta}_{\text{p}}$ platform kinematics aiming for a good emulation of sensed acceleration for the driver, see Eq. 4. Additionally, translational and rotational displacements can be defined within the 27x1 vector

$$\mathbf{u}_{\text{udp,p}}^{K_{SAE}} = \left[\begin{array}{ccccccc} \mathbf{v}_{\text{veh}} & \mathbf{a}_{\text{veh}} & \mathbf{R}_{\text{IR}} & \dot{\boldsymbol{\beta}}_{\text{veh}} & \ddot{\boldsymbol{\beta}}_{\text{veh}} & \mathbf{s}_{\text{p,man}} & \boldsymbol{\beta}_{\text{p,man}} \end{array} \right]^T \tag{3}$$

which is transferred to the platform software using the generic udp-interface of SIMCORDX [17]. However, the input vectors must be transformed into the platform coordinate system to avoid false direction convention regarding the lateral and vertical axis. The input vector consists of the 3x1 vectors of the vehicle states: velocity $\mathbf{v}_{\text{veh}}$, acceleration (without gravity component) $\mathbf{a}_{\text{veh}}$, angular velocity $\dot{\boldsymbol{\beta}}_{\text{veh}}$ and angular acceleration $\ddot{\boldsymbol{\beta}}_{\text{veh}}$, the 9x1 vector with entries of the rotational matrix and the 3x1 vectors of manual defined translational $\mathbf{s}_{\text{p,man}}$ and rotational $\boldsymbol{\beta}_{\text{p,man}}$ displacement of the platform.

Besides the activation with classical MCA, the setup allows the direct definition of platform trajectories using the vectors $\mathbf{s}_{\text{p,man}}$ and $\boldsymbol{\beta}_{\text{p,man}}$. Also, the superposition of MCA and manual positioning is enabled, which allows the optimization of maximal displacements in specific scenarios, i.e. by adding a constant offset to the neutral position of one or more axes.

Due to the small translational movement corridor, the Motion Cueing Algorithms use special approaches like washout filtering and tilt coordination [18], to ensure enhanced driving sensation without violating kinematic limits. The tilt coordination approach uses the assumption that the human vestibular system in the inner ear - responsible for the equlibrium sense - cannot distinguish translational accelerations from rotational displacements in a gravitational field [18], see Fig. 4. Classical MCAs using tilt coordination separate the acceleration signals into high and low-frequency parts. While only the high-frequency parts of the translational accelerations are performed by translational trajectories of the motion platform $\mathbf{s}_{\text{p}}$, long-term accelerations are imitated by rotational displacements $\boldsymbol{\beta}_{\text{p}}$.

$$\boldsymbol{\zeta}_p(t) = \begin{pmatrix} \mathbf{s}_{\text{p}}(t) \\ \boldsymbol{\beta}_{\text{p}}(t) \end{pmatrix} = f_{\text{MC}}(\boldsymbol{\zeta}_{\text{veh}}(t)) = f_{\text{MC}} \begin{pmatrix} \mathbf{a}(t) \\ \boldsymbol{\beta}(t) \\ \dot{\boldsymbol{\beta}}(t) \end{pmatrix}_{\text{veh}} \tag{4}$$

In Fig. 4 the tilt coordination approach is shown. The sensed acceleration is written as specific forces [16]. Dependant on the changed orientation of the simulator $\boldsymbol{\beta}_{\text{p,TC}}$ due to the TC approach, following specific force can

be calculated:

$$\begin{aligned}\mathbf{f}_{\mathrm{TC}} &= \mathbf{R}_{K_{\mathrm{TC}}K_0} \cdot \mathbf{g} = (\mathbf{R}_{K_0K_{\mathrm{TC}}})^T \cdot \mathbf{g} = (\mathbf{R}_{\mathrm{xy'z''}})^T \cdot \mathbf{g} \\ &= \begin{bmatrix} * & * & sin(\theta_{\mathrm{TC}}) \\ * & * & sin(\phi_{\mathrm{TC}})cos(\theta_{\mathrm{TC}}) \\ * & * & cos(\phi_{\mathrm{TC}})cos(\theta_{\mathrm{TC}})) \end{bmatrix} \cdot \begin{bmatrix} 0 \\ 0 \\ -g \end{bmatrix} = \begin{bmatrix} -sin(\theta_{\mathrm{TC}}) \\ -sin(\phi_{\mathrm{TC}})cos(\theta_{\mathrm{TC}}) \\ -cos(\phi_{\mathrm{TC}})cos(\theta_{\mathrm{TC}})) \end{bmatrix} g \end{aligned} \tag{5}$$

The rotation angles ϕ_{TC} and θ_{TC} are not represented by the visual feedback. They represent only the difference between total platform rotation and rotations due to rotational displacements of the vehicle model $\theta_{\mathrm{p,veh}}$

$$\boldsymbol{\beta}_{\mathrm{TC}} = \boldsymbol{\beta}_{\mathrm{p,total}} - \boldsymbol{\beta}_{\mathrm{p,veh}}. \tag{6}$$

The yaw angle ψ does not contribute to the specific force due to its orthogonality to the gravitational vector $\mathbf{g}$. The total specific force is written as

$$\mathbf{f}_{\mathrm{total}} = \mathbf{a} + \mathbf{f}_{\mathrm{TC}}. \tag{7}$$

Low-frequented translational accelerations can be emulated by rotating the platform. However, rotations of the platform lead to translational velocities of the test person's head and simulator

$$\begin{aligned}\mathbf{v}_{\mathrm{TC,h}} &= \dot{\boldsymbol{\beta}}_{\mathrm{p}} \times \mathbf{r}_{\mathrm{OP,h}} \\ \mathbf{v}_{\mathrm{TC,p}} &= \dot{\boldsymbol{\beta}}_{\mathrm{p}} \times \mathbf{r}_{\mathrm{OP,p}}\end{aligned} \tag{8}$$

until the desired position is reached. Dependent on the distance between pivot point and platform centre point $\mathbf{r}_{\mathrm{OP,p}}$ or pivot point and head of the test person $\mathbf{r}_{\mathrm{OP,h}}$, the transient rotations result in different translation movements of driver's head $\mathbf{s}_{\mathrm{TC,h}}$ and platform $\mathbf{s}_{\mathrm{TC,p}}$, see Fig. 4.

To fulfill the TC approach, a rotational centre in the middle of the head ($\mathbf{r}_{\mathrm{OP,h}} = 0$) should be used. In this case, the vestibular system of the test person only recognizes the rotational displacement interpreted as the desired long-term accelerations and no additional translational acceleration in result of the transient tilt coordination rotations. However, it is not possible to minimize both the distance between the pivot point and the platform $\mathbf{r}_{\mathrm{OP,p}}$ and the head of the test person $\mathbf{r}_{\mathrm{OP,h}}$ at the same time. While the translational accelerations of the head $\mathbf{a}_{\mathrm{TC,h}}$ directly influence the quality of the MCA, the translation displacements $\mathbf{s}_{\mathrm{TC,p}}$ which have to be performed by the platform

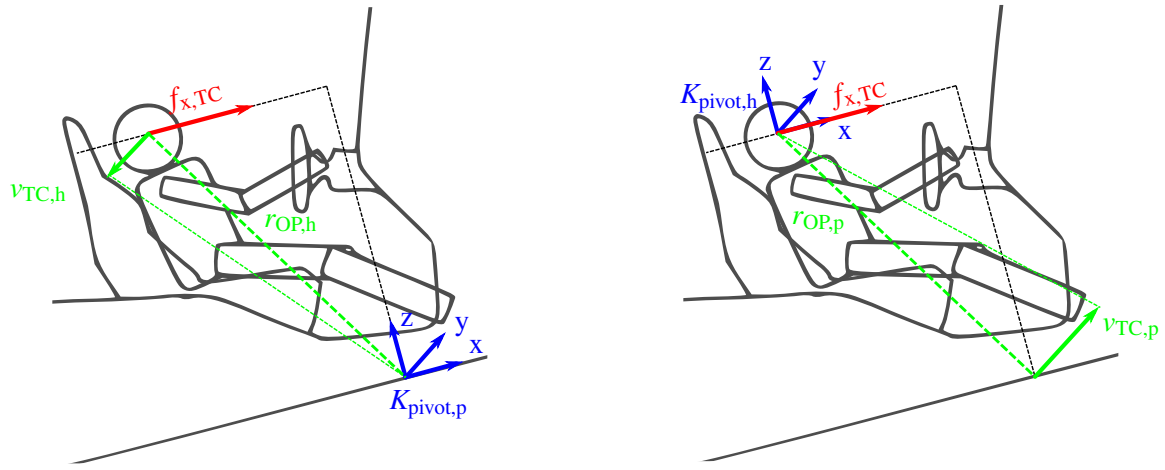

Fig. 4: Influence of the pivot point definition on the tilt coordination approach shown in an acceleration scenario in longitudinal direction: The specific force in longitudinal direction $\mathbf{f}_{\mathrm{x,TC}}$ which is related to the perceived translational acceleration of the driver is dependent on the orientation of the simulator but independent of the defined pivot point of the platform. Left: Default position of the pivot point $K_{\mathrm{pivot,p}}$ at the platform center point. No additional translational velocities $\mathbf{v}_{\mathrm{TC,p}}$ have to be performed by the platform. Due to the non-zero position vector $\mathbf{r}_{\mathrm{OP,h}}$ between pivot point and head, unwanted translational velocities $\mathbf{v}_{\mathrm{TC,h}}$ are applied during rotations. Right: If the pivot point $K_{\mathrm{pivot,h}}$ is placed to the driver's head, the undesirable head velocities disappear ($\mathbf{v}_{\mathrm{TC,h}} = 0$). In this case, the platform has to perform additional velocities $\mathbf{v}_{\mathrm{TC,p}}$ to enable the rotations around the desired pivot point, see [16].

to ensure the TC further reduce the translational movement space of the platform. The quality of the calculated and performed motion cues can be rated with mathematical models of the vestibular system, comparing the sensed accelerations of the driver in the simulator and those in a real car representing by the states of the vehicle model, see Section 2.4.2. Besides the calculation of adequate platform kinematics with MCAs, SIMCORDX enables the control of the six motor devices of the stewart platform

$$\zeta_{\mathrm{eng}}(t) = \begin{pmatrix} \mathbf{i}_{\mathrm{eng},1}(\mathbf{t}) \\ \cdots \\ \mathbf{i}_{\mathrm{eng},6}(\mathbf{t}) \end{pmatrix} = f_{\mathrm{eng}}(\zeta_{\mathrm{p}}(t), \zeta_{\mathrm{eng}}(t)) \tag{9}$$

to perform the desired trajectories.

2.4.2 Vestibular System

The quality of calculated or performed motion cues can be rated with mathematical models of the vestibular system, comparing the sensed accelerations of the driver in the simulator and those in a real car or the vehicle model respectively [16]. In Fig. 5 the approach of sensational error between the perception of accelerations inside the virtual vehicle model $\tilde{a}_{\mathrm{V}}$ and those inside the DiL-simulator provided by the platform kinematics $\tilde{a}_{\mathrm{p}}$ is depicted. The accelerations applied to the test person inside the simulator can be predicted by performing Motion Cueing and using a dynamical model of the motion platform. Alternatively, the load on the driver can be detected by the Motion Capture System, see Section 3.1. For future investigations and offline parameter optimization, a dynamical model of the motion platform is aimed for.

The mathematical models of the human vestibular system use transfer functions to scale the signals dependently on their frequency. Therefore, the models account for the frequency-dependent perception abilities of the vestibular system. Additionally, the specific forces of the TC-rotations are considered for the estimation of sensed translational accelerations. By including the thereby predicted perception error into cost functions, parameter optimization, as well as enhanced strategies for Motion Cueing with optimal control approaches, are enabled.

2.4.3 Vehicle Vibrations

Vehicle vibrations in real driving conditions, like those induced by engine and road roughness, can be imitated by activating the platform, the bass-shaker at the back of the seat or the force-feedback wheel. Due to the high inertias, vibrations should not primarily be performed by the platform. Therefore appropriate states of the vehicle model $\zeta_{\mathrm{v,so}}$, like velocity or engine speed, are transferred to the software SUPERCOLLIDER via open sound control and used for the sound synthesis. Via the sound system and especially the bass shaker the driver is exposed to vibrations

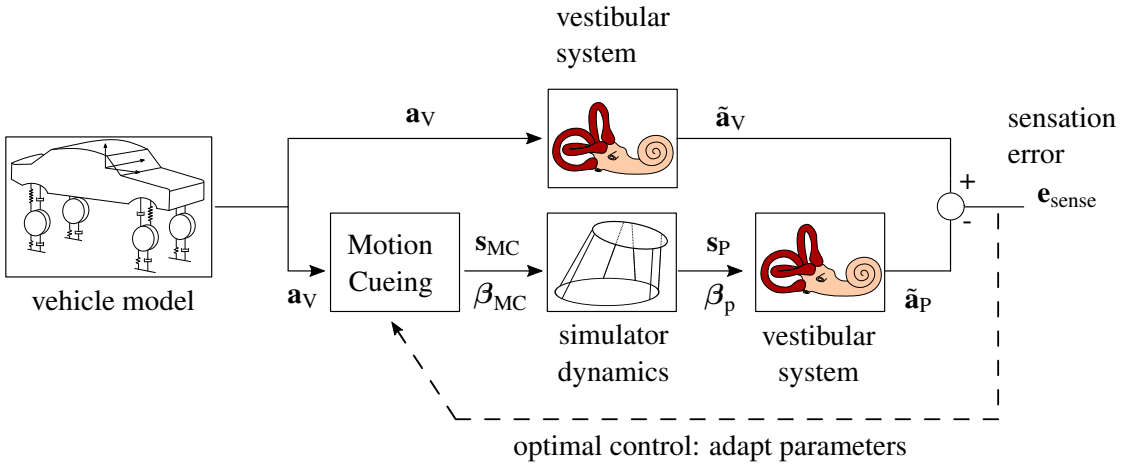

Fig. 5: Workflow for the quality estimation of Motion Cueing Algorithms using models of the human vestibular system. The sensation error is defined as difference between the accelerations perceived in the vehicle model and those perceived through the kinematics provided by the platform, see [19].

which enhance the driving immersion and reduce the perception ability of the driver to detect false motion cues [16].

2.4.4 Force-Feedback Steering Wheel

In addition to the feedback of the vehicle dynamics via the platform kinematics, the interaction with the steering wheel contributes to the immersion quality. Velocity-dependent steering torques, vibrations induced by road roughness and functionalities of driver assistance systems can be emulated by the FANATEC force-feedback steering wheel installed in the DiL-simulator.

The force-feedback functionalities are provided by two main methods implemented in the PRESCAN interface, which are spring and periodic effects. Steering torques are applied by linear spring characteristics according to:

$$T_{\text{steer}} = c_{\text{spring}}(\phi_{\text{steer}}(t) - \phi_{\text{center}}(t)) \tag{10}$$

with a linear stiffness c_{spring} defined on the displacement between the steering wheel angle $\phi_{\text{steer}}(t)$ and defined steering center angle ϕ_{center}. By defining a specific trajectory as input of the center angle ϕ_{center}, active steering interaction is enabled. Vibrations can be induced by defining type and intensity of the periodic excitation. Driver assistance systems like lane-departure warning and lane change assistant can be emulated with the force-feedback wheel. For emergency lane-change applications, it can be useful to decouple the steering wheel from the actual steering action to avoid hand injuries. This decoupling is similar to steer-by-wire approaches of modern real-world vehicles.

3 Measurement chain

With the presented DiL-simulator, test persons can be exposed to virtual driving scenarios in a safe environment. To analyze the drivers' behavior in the DiL-simulator during Pre-Crash situations, their kinematics as well as the muscle activations are monitored. The **kinematics** are tracked by a motion capture system from OPTITRACK using computer stereo vision with reflexive infrared markers and four cameras of the type Prime 13W. The cameras with internal image processing enable low latencies and framerates up to 240 Hz with minimized data transfer in the camera network.

Additional to the kinematics of the driver, the **muscle activation** levels are tracked by electromyography measures (EMG). This muscle information is inevitable to determine muscle activation and co-contraction levels at different joints in more detail. By the simultaneous contraction of agonist and antagonist, the stiffness properties of a joint can be increased. In crash simulations with HBMs these co-contraction levels can be used to adjust stiffness properties to replicate different states of pretension of the occupants, which show a high influence on the injury outcome [20]. In contrast to dummy models, active HBMs can vary their stiffness parameters during runtime. Additionally, useful information on the muscle activation strategies of human drivers can be collected and used for development of improved muscle controllers.

3.1 Motion Capture with Stereo Vision

The Optitrack camera system is stationary fixed in the lab to avoid vibrations and relative displacements between the several cameras which would lead to errors in marker tracking. The software package MOTIVE allows the reconstruction of 3D-positions of reflexive markers. It uses the information obtained by the four cameras installed in the prior calibrated setup. Additionally to the position detection of single markers, rigid bodies can be defined using three or more markers which show no relative displacements during the tests. Once defined, they are automatically detected by MOTIVE due to their unique marker configuration. The benefit of using rigid bodies instead of single markers is that the labeled position and orientation of the elements can be easily accessed without any manual selection.

To reconstruct the driver kinematics reflexive markers are placed on the surface of the test person at points with anatomical relevance, like joints or bones, see 6. The obtained time-curves of the joint-angles and relative

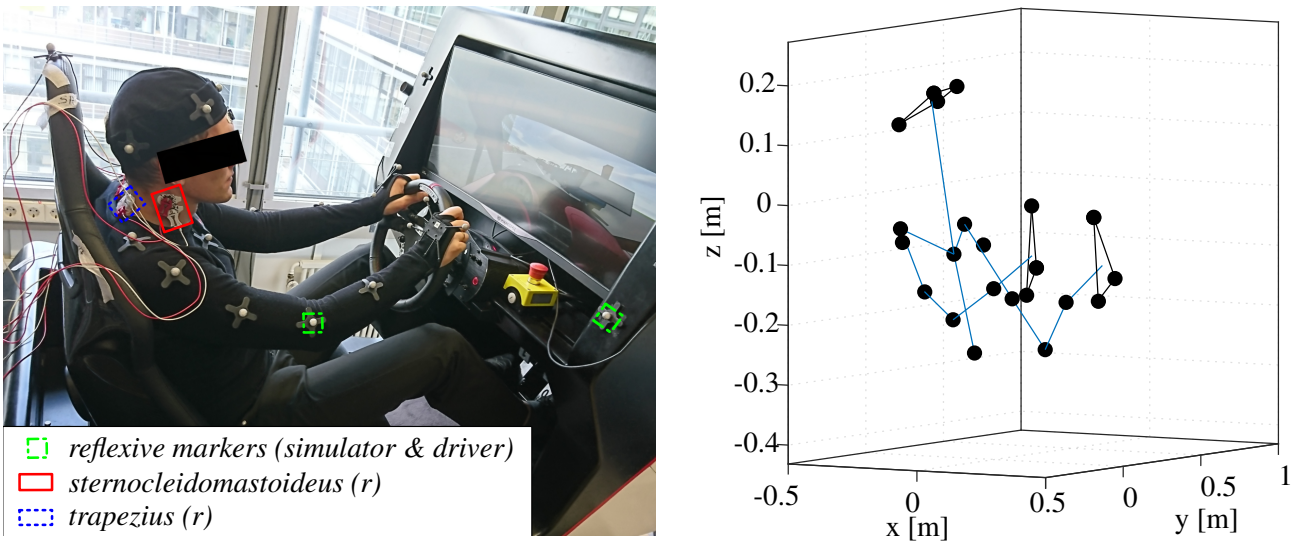

Fig. 6: Sensor placement and marker based skeleton reconstruction. Left: Setup with reflexive markers, i.e. elbow marker (green dash-dotted) and EMG sensors *right sternocleidomastoideus* (red) and *right trapezius* (blue dashed). Right: Reconstructed model of the skeleton based on the position data of the markers.

displacements document the executed movement of the driver. Besides the absolute kinematics of the driver, also the movements performed relative to the simulator are of special interest. To transform absolute kinematics into relative ones, the simulator itself is also tracked by the camera system enabling transformations in the post-processing.

3.1.1 Platform Kinematics

To detect the motion of the platform and simulator, markers are placed on the surface of the platform and defined as rigid body in MOTIVE. With the tracked kinematics of the platform, the Motion Cueing Algorithms can be validated. Additionally, the investigation of relative motions between driver and simulator are enabled as well as the definition of the load applied to the driver by the motion platform.

3.1.2 Marker Placement and Skeleton Model

For an efficient investigation of the experimental tests, the work-flow of the marker detection and skeleton reconstruction should be as automatized as possible. For the post-processing, the markers should be assigned automatically to the corresponding skeleton points of the surrogate model. Therefore, rigid bodies are used as orientation and starting points. These elements are detected automatically by the MOTIVE software if once defined. In the experimental tests the platform, simulator, head and both hands are defined as rigid bodies using three (hands) or four markers (head, simulator, platform).

The markers are allocated to the skeleton parts using mainly distance measures scaled by the height of the test person. Therefore, the skeleton reconstruction gets more robust by adjusting only one parameter per test person. The hands serves as starting points of the assignment process. In Fig. 6 on the left the marker placement of the setup is shown. On the right the corresponding reconstructed skeleton can be seen. The defined rigid bodies of the skeleton are illustrated as black triangles or squares respectively. Time-series of joint angles as well as displacements of specific skeleton points can be determined using the reconstructed skeleton model.

3.1.3 Transformation

Based on the tracked position and rotations of the simulator, a body-fixed coordinate system K_S is defined. Homogeneous coordinates and corresponding transformation matrices are used to calculate the relative kinematics of the driver. Both translational displacements $\mathbf{z}_{KK_S}$ and rotations $\mathbf{R}_{KK_S}$ between the two coordinate systems are defined

using a 4x4 matrix. The matrix $\mathbf{C}_{KK_S}$ transforms the coordinates of the local coordinate system K_S into the inertial system K while $\mathbf{C}_{K_SK}$ ensures the back transformation.

$$\mathbf{C}_{\mathrm{KK'}} = \left[\begin{array}{c|c} \mathbf{R}_{KK_S} & \mathbf{z}_{KK_S} \\ \hline \mathbf{0} & 1 \end{array}\right] \qquad \mathbf{C}_{\mathrm{K'K}} = \left[\begin{array}{c|c} \mathbf{R}_{KK_S}^T & -\mathbf{R}_{KK_S}^T \cdot z_{KK_S} \\ \hline \mathbf{0} & 1 \end{array}\right] \tag{11}$$

The relative coordinates of markers $\mathbf{r}_{\mathrm{i}}^{K_S}$ are calculated by

$$\left[\begin{array}{c} \mathbf{r}_{\mathrm{i}}^{K_S} \\ 1 \end{array}\right] = \mathbf{C}_{K_SK} \left[\begin{array}{c} \mathbf{r}_{\mathrm{i}}^{K} \\ 1 \end{array}\right] \tag{12}$$

Investigations of special interest could be done using:

- absolute coordinates $\mathbf{r}_{\mathrm{OP_i}}^{K}$ to validate the Motion Cueing Algorithms or to define the load of the driver during Pre-crash scenarios like head accelerations, or
- relative coordinates $\mathbf{r}_{\mathrm{SP_i}}^{K_S}$ to characterize the kinematics of relevant skeleton points like translational and rotational head displacements.

3.2 Electromyography

Surface electromyografic (SEMG) measurements are performed to measure the activity of specific muscles stabilizing the head when driving. SEMG data were recorded from the *sternocleidomastoideus* and the *trapezius* muscles using bipolar Ag/AgCl electrodes with an inter-electrode distance of 20 mm, see 6. The conductivity of the skin was improved according to the recommendations of SENIAM [21]: the skin was shaved, abraded and cleaned with alcohol. The target muscles were located based on the recommendations of [22]. After skin preparation three maximal voluntary contractions (MVC) were performed.

3.2.1 Data analyse

The SEMG data were recorded using a Biopac MP160 system (Biopac Systems, Goleta, USA) with a sample rate of 4 kHz, pre-amplified (5000) and bandpass filtered (10 - 500 Hz). Subsequently, the data were rectified and a root mean square filter over 250 samples was applied. The SEMG data during the measurements of the single pre-crash scenarios (Tab. 1) were normalized to the maximal amplitude of the MVC and thus can be interpreted as the degree of muscle activation.

3.3 Synchronization

To synchronize the data detected by several measurement systems and the Driver-in-the-Loop simulation during runtime, following control commands are used:

- electrical trigger signal provided by an Arduino UNO R3 for EMG synchronization
  $writeDigitalPin(arduino,'D8',1)$,
- remote control of Optitrack camera system
  $natnet.startRecord$,
- udp stream to SIMCORDX and SUPERCOLLIDER
  $udp\_send(\mathbf{u}_{\mathrm{udp,p}}^{K_{\mathrm{SAE}}})$; $osc\_send(v_{\mathrm{m}}, v_{\mathrm{veh}})$.

In the initialization phase of the simulation the connections to the Arduino board and the additional software tools running on the second computer are initialized. If the trigger criterion in the DiL-simulation, i.e. distance measure to the crash location, is fulfilled, the subsystems are triggered. An electrical trigger signal is sent to the

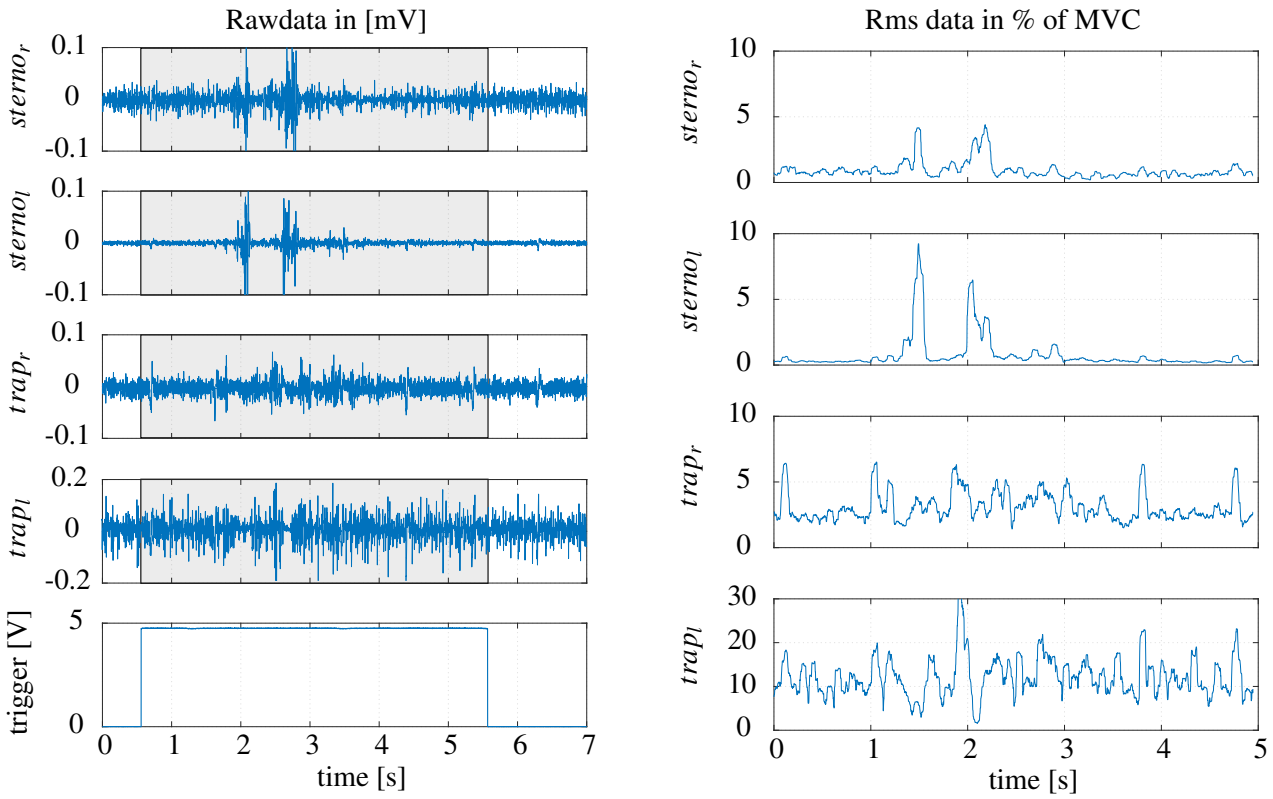

Fig. 7: Processing of the EMG signals: rawdata with trigger signal (left) and transformed root-mean-square data as percentage of the MVC (right).

EMG measurement system using a digital Output of the Arduino board which is connected to the EMG measurement system via a bnc cable. This recorded electrical 5 V signal gives the EMG signals a specific timestamp relative to the DiL-simulation. Simultaneously, the Optitrack software Motive running on the second computer with activated server application is triggered via the NATNET SDK using network communication. Investigations show that the latencies of the cameras and the software lead to missing data of the first 5 ms. To address this latency, the curves are shifted 5 ms backward. As a result of the synchronization the obtained data – both EMG and kinematics – have a unified time axis. Therefore, interrelations between kinematics and muscle activation can be found. Increased muscle activity detected in EMG data can be allocated to the specific kinematics of the driver and simulator, see Fig. 9. Muscle onset detection, i.e. with methods presented in [23], are enabled.

4 Experimental Tests

First experimental tests are made to show the performance of the complete setup. The simulator and platform are equipped with passive markers to detect their kinematics during the tests. Different platform activation strategies can be used to emulate the kinematics of the vehicle model. The tilt coordination approach uses additional rotations which are not physically performed by the vehicle model. To investigate this topic, we plan to compare platform activation with and without tilt coordination. Also the kinematics of the driver are reconstructed using the 3D positions of the markers attached to the test person.

4.1 Platform Performance

To show the performance of the simulator, we use the Optitrack system to track its kinematics. By attaching four reflexive markers directly on top of the platform and defining them as rigid body, we get straightly the translational and rotational trajectories of the platform. We use the RPY-transformation for the rotation export. Dependent on the choice of the MCAs and their parametrization, superposed rotational displacements are applied to the driver

Tab. 1: Overview of the performed Pre-Crash scenarios - emergency brake and evasive maneuver.

Pre-Crash scenario	initial speed	type of intervention	result of maneuver
I) emergency brake	50 km/h	maximal brake pressure	stopping distance: 10.5 m
II) single lane-change	50 km/h	steering trajectory with $\phi_{\text{steer,max}} = 67.5°$	lateral distance: 4 m

to emulate translational accelerations, i.e. see platform rotations in Fig. 9 (right top row). The influence of these additional rotations can be investigated in further studies.

4.2 Test Schedules

For the experimental tests, two driving scenarios are defined. One single lane-change maneuver and one with an emergency brake, see Fig.8. In Tab. 1 the most important parameters of the maneuvers are depicted. To increase the reproducibility and to facilitate the comparisons between the experiments, the only task of the driver is to hold the track. The DiL-vehicle accelerates and brakes on its own. The Pre-Crash intervention is performed by pre-defined functions for steering or pedal positions emulating ADASs. To avoid unnecessary complexity, we use one simulation environment and change only the intervention of the emulated driver assistance system. The environment, as well as the car introducing the episode, are identical. During one take, the subject is requested to hold a predefined head position according to the test protocol. Besides the standard view to the front, the viewing direction are changed to the very right or very left, emulating for example a safety view before a lane-change maneuver. This results in constant, initial head rotations of approximately 90°. The experimental data shall enable further investigations of the influence of head rotations due to changed viewing directions. To prevent adaptation of the test person, the specified scenarios are ordered randomly. A change of the scenarios can be done directly in the SIMULINK model, enabling a smooth test procedure. Each configuration is performed three times to enable statistically investigations. Altogether, we did 2 maneuvers * 3 viewing directions * 3 takes = 18 takes for each of the three test persons. Additionally to the scenarios, maximum contraction levels of each test person are defined by isometrical tests beforehand, see Section 3.2.

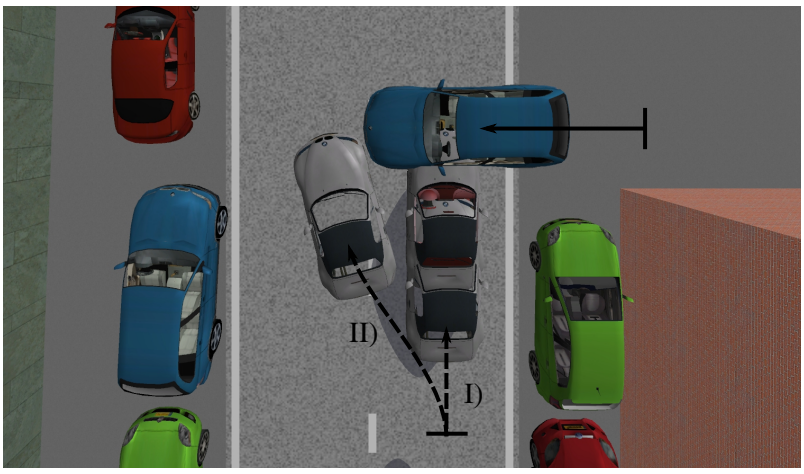

Fig. 8: Top-view on the Pre-Crash scenarios modeled in PRESCAN. The gray DiL-vehicle performs I) emergency brake or II) single lane-change maneuver to avoid crash with blue car crossing the lane from the right.

5 Results

To depict possible investigations, the obtained data of one subject performing the emergency brake scenario with viewing point to the front is exemplary investigated. In Fig. 9 the most relevant platform and head kinematics as well as the corresponding EMG data of the neck muscles are shown. The head motion is quite different in the three emergency brake scenarios despite almost identical kinematics of the platform, see first and second row in Fig. 9. The lowest head displacement was found for take 1 (blue line, second row). This could be explained by a higher baseline *trapezius* activation during take 1 (blue line, fourth row). In contrast to the *trapezius*, the EMG data of the *sternocleidomastoideus* (third row) show distinct muscle activation patterns with consistent muscle onset about 200 ms after start of the platform action referred to the brake event. We found submaximal sternocleidomastoideus muscle activation up to 10% MVC. For the selected subject, muscle activations of the left side head muscles are higher than those of the right side.

Further investigations, like statistical analysis and comparisons between different subjects and scenarios will be given in later publications.

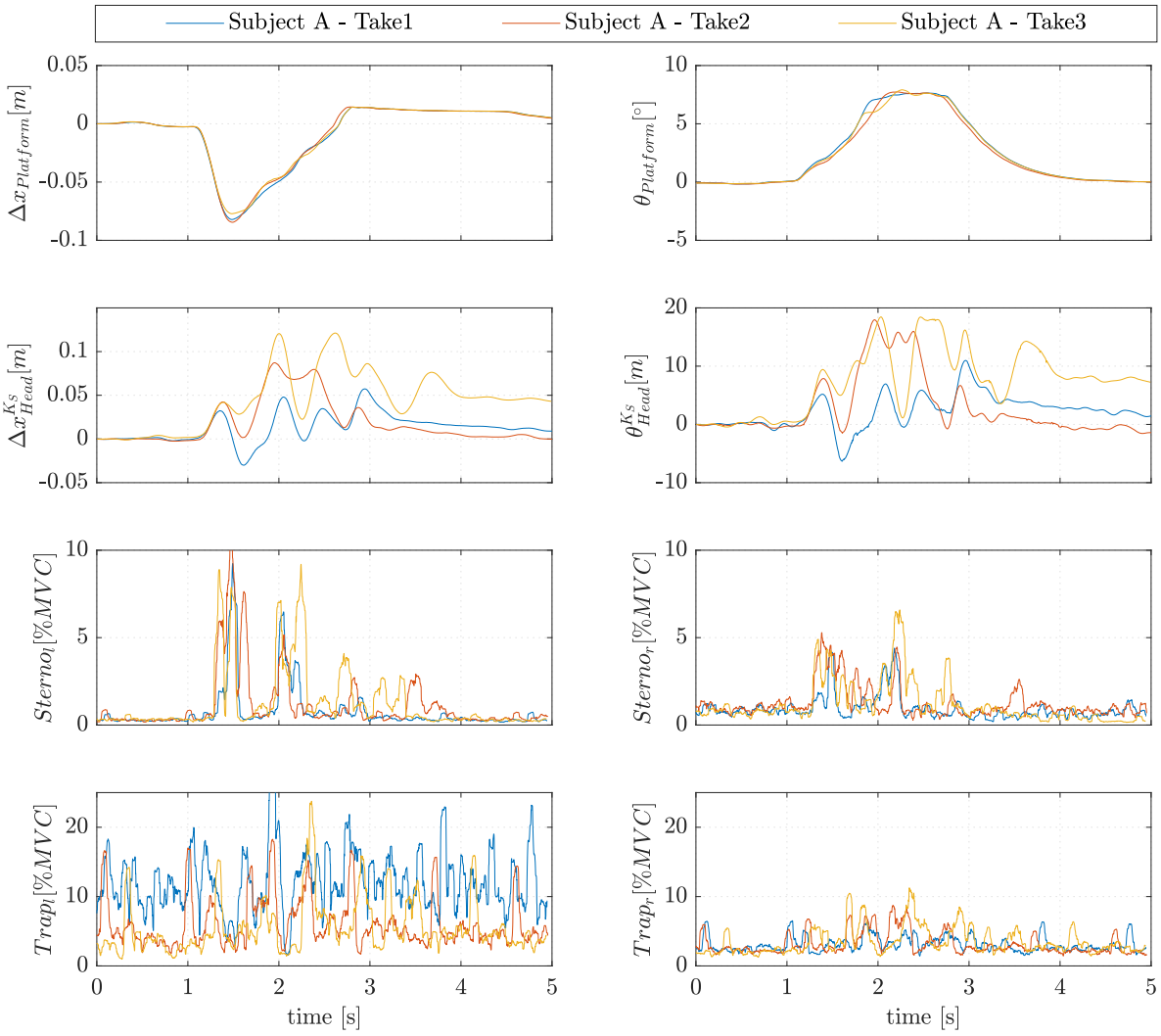

Fig. 9: Synchronized capture data of one test person performing three times emergency brake scenario. 1.line: absolute platform trajectories, translational displacements (left) and rotational displacements (right); 2.line: relative head displacements x-translation (left) and rotational displacements around y_{head}-axis; 3.line EMG data of *sternocleidomastoideus* left and right; 4.line EMG data of *trapezius* left and right.

6 Conclusions

The presented setup of a Driver-in-the-Loop simulator allows investigations of driver behavior in Pre-Crash scenarios with and without interaction of driver assistance systems. The synchronized observation data enables the detection of activation patterns in the EMG data with respect to the kinematics of platform and reconstructed skeleton points. The provided data obtained by the monitoring devices will be used to improve the biofidelity of active HBMs and their muscle activation strategies. Advanced muscle materials with more physiological properties and activation possibilities, e.g. [24, 25, 26, 27], will enable a more human-like behavior of the occupant models after accurate validation processes. These advanced active HBMs, validated for Pre-Crash simulations, can serve as a tool for enhancing integrated safety systems and clear the way for automated traffic with improved real-world safety.

In further studies, we want to investigate and analyze the obtained data concerning activation levels and time of muscle onsets, see [23]. Furthermore, the driver immersion shall be enhanced by improving visualization - via a head-mounted display (HMD) and increased realism in scenarios - or by using enhanced driving simulators or even real cars. The results of different setups could be compared to estimate the accuracy of the investigations with an academic-scale simulator.

Acknowledgements

The authors would like to thank the state Baden-Wuerttemberg and the German Research Foundation (DFG) through for the financial support of the project within the Juniorprofessor program and the Exzellenzcluster 310 Simulation Technology at the University of Stuttgart. The companies TASS international, CKAS, Silkroad/Vischer and EST for the discount on soft- and hardware products. Additionally, we want to thank Christian Kleinbach, Bünyamin Tezcan, Julian Fuhrer, Pascal Ziegler and Peter Schöler for the support at commissioning the DiL-simulator. This study was supported by the ”Research Seed Capital“ of the Ministry of Science, Research and Arts Baden-Wuerttemberg as well as the University of Stuttgart.

References

[1] R. Schoeneburg, K.-H. Baumann, and M. Fehring, "The efficiency of PRE-SAFE systems in pre-braked frontal collision situations," in *Proceedings of the 22nd International Technical Conference on the Enhanced Safety of Vehicles*, (Washington, D.C.), pp. 1–11, 2011.

[2] L. Feller, C. Kleinbach, J. Fehr, and S. Schmitt, "Incorporating muscle activation dynamics into the Global Human Body Model," in *Proceedings of the IRCOBI Conference*, (Malaga, Spain), 2016.

[3] M. Lindman, I. Isaksson-Hellman, and J. Strandroth, "Basic numbers needed to understand the traffic safety effect of automated cars," in *Proceedings of the IRCOBI Conference*, (Antwerp, Belgium), 2017.

[4] J. Östh, K. Brolin, J. M. Ólafsdóttir, J. Davidsson, B. Pipkorn, L. Jakobsson, F. Törnvall, and M. Lindkvist, "Muscle activation strategies in human body models for the development of integrated safety," in *24th International Technical Conference on the Enhanced Safety of Vehicles*, no. 15-0345, (Gothenburg, Sweden), 2015.

[5] S. Beeman, A. Kemper, M. Madigan, C. Franck, and S. Loftus, "Occupant Kinematics in Low-speed Frontal Sled Tests: Human Volunteers, Hybrid III ATD, and PMHS," *Accident Analysis & Prevention*, vol. 47, pp. 128–139, 2012.

[6] S. Kirschbichler, P. Huber, A. Prüggler, T. Steidl, W. Sinz, C. Mayer, and G. A. D'Addetta, "Factors influencing occupant kinematics during braking and lane change maneuvers in a passenger vehicle," in *Proceedings of the IRCOBI Conference*, (Berlin, Germany), pp. 614–625, 2014.

[7] J. M. Olafsdottir, J. Östh, J. Davidsson, and K. Brolin, "Passenger kinematics and muscle responses in autonomous braking events with standard and reversible pre-tensioned restraints," in *Proceedings of the IRCOBI Conference*, no. IRC-13-70, (Gothenburg, Sweden), pp. 602–617, 2013.

[8] M.-P. Pacaux-Lemoine, H. Morvan, F. Robache, J. Floris, and P. Drazetic, "Driving simulator use for pre-crash tests," in *DSC North America*, (Orlando), November 2005.

[9] A. Hault-Dubrulle, F. Robache, M.-P. Pacaux, and H. Morvan, "Determination of pre-impact occupant postures and analysis of consequences on injury outcome. part i: A driving simulator study," *Accident Analysis & Prevention*, vol. 43, no. 1, pp. 66 – 74, 2011.

[10] Euro NCAP, "2020 Road Map – European New Car Assessment Programme," tech. rep., Euro NCAP, Leuven, Belgium, March 2015.

[11] Euro NCAP, "2025 Road Map – European New Car Assessment Programme," tech. rep., Euro NCAP, Leuven, Belgium, 2017.

[12] TASS International, *PRESCAN-Manual v 8.2.0*. Rijswijk, Netherlands, 2017.

[13] T. Shiiba, J. Fehr, and P. Eberhard, "Flexible multibody simulation of automotive systems with non-modal model reduction techniques," *Vehicle System Dynamics*, vol. 50, no. 12, pp. 1905–1922, 2012.

[14] CKAS, *User Manual CKAS Motion System Generation III ICD*. Melbourne, Australia, 2015.

[15] H. Schmieder, K. Nagel, and H.-P. Schoener, "Enhancing a driving simulator with a 3D stereo projection system," in *Proceedings of the Driving Simulator Conference*, (Stuttgart, Germany), 2017.

[16] M. Fischer, *Motion-Cueing-Algorithmen für eine realitätsnahe Bewegungssimulation*. PhD thesis, Braunschweig, Germany, 2009.

[17] CKAS, *User Manual CKAS Generic UDP Interface Manual*. Melbourne, Australia, 2013.

[18] M. A. Nahon and L. D. Reid, "Simulator motion-drive algorithms - a designer's perspective," *Journal of Guidance, Control, and Dynamics*, vol. 13, pp. 356–362, 1990.

[19] C.-I. Huang and L.-C. Fu, "Human vestibular system based optimal washout filter design on motion platform constraint," in *Proceedings of the 8th IFAC Symposium on Robot Control*, (Bologna, Italy), pp. 394 – 399, 2006.

[20] R. Meijer, H. Elrofai, J. Broos, and E. van Hassel, "Evaluation of an active multi-body human model for braking and frontal crash events," in *Proceedings of the 23rd International Technical Conference on the Enhanced Safety of Vehicles*, (Seoul, Republic of Korea), pp. 1–12, NHTSA, 2013.

[21] H. J. Hermens, B. Freriks, C. Disselhorst-Klug, and G. Rau, "Development of recommendations for semg sensors and sensor placement procedures," *Journal of Electromyography and Kinesiology*, vol. 10, no. 5, pp. 361 – 374, 2000.

[22] M. Barbero, R. Merletti, and A. Rainoldi, *Atlas of Muscle Innervation Zones: Understanding Surface Electromyography and Its Applications*. Milan, Italy: Springer, 2012.

[23] G. Staude, C. Flachenecker, M. Daumer, and W. Wolf, "Onset detection in surface electromyographic signals: A systematic comparison of methods," *EURASIP Journal on Advances in Signal Processing*, 2001.

[24] C. Kleinbach, O. Martynenko, J. Promies, D. F. B. Haeufle, J. Fehr, and S. Schmitt, "Implementation and validation of the extended Hill-type muscle model with robust routing capabilities in LS-DYNA for active human body models," *BioMedical Engineering OnLine*, vol. 16, p. 109, 2017.

[25] J. Fehr, F. Kempter, C. Kleinbach, and S. Schmitt, "Guiding strategy for an open source Hill-type muscle model in LS-DYNA and implementation in the upper extremity of a HBM," in *Proceedings of the IRCOBI Conference*, (Antwerp, Belgium), 2017.

[26] T. Siebert, N. Stutzig, and C. Rode, "A Hill-type muscle model expansion accounting for effects of varying transverse muscle load.," *Journal of biomechanics*, vol. 66, pp. 57–62, 2018.

[27] T. Heidlauf, T. Klotz, C. Rode, T. Siebert, and O. Röhrle, "A continuum-mechanical skeletal muscle model including actin-titin interaction predicts stable contractions on the descending limb of the force-length relation," *PLOS Computational Biology*, vol. 13, no. 10, pp. 1–25, 2017.